



**HAL**  
open science

## Current redistribution during inhomogeneous quench of 2G HTS tapes

Alexandre Zampa, Christian Lacroix, Arnaud Badel, Frédéric Sirois, Pascal  
Tixador

► **To cite this version:**

Alexandre Zampa, Christian Lacroix, Arnaud Badel, Frédéric Sirois, Pascal Tixador. Current redistribution during inhomogeneous quench of 2G HTS tapes. *Superconductor Science and Technology*, 2022, 35 (9), pp.095003. 10.1088/1361-6668/ac7c96 . hal-04440406v2

**HAL Id: hal-04440406**

**<https://hal.science/hal-04440406v2>**

Submitted on 6 Feb 2024

**HAL** is a multi-disciplinary open access archive for the deposit and dissemination of scientific research documents, whether they are published or not. The documents may come from teaching and research institutions in France or abroad, or from public or private research centers.

L'archive ouverte pluridisciplinaire **HAL**, est destinée au dépôt et à la diffusion de documents scientifiques de niveau recherche, publiés ou non, émanant des établissements d'enseignement et de recherche français ou étrangers, des laboratoires publics ou privés.

# Current redistribution during inhomogeneous quench of 2G HTS tapes

Alexandre Zampa<sup>1</sup>, Christian Lacroix<sup>2</sup>, Arnaud Badel<sup>1</sup>, Frédéric Sirois<sup>2</sup> and Pascal Tixador<sup>1</sup>

<sup>1</sup> Univ. Grenoble Alpes, CNRS, GRENOBLE INP\*, G2ELab – Institut Néel, 38000 Grenoble FRANCE

<sup>2</sup> Department of Electrical Engineering, Polytechnique Montréal, Montréal, QC, H3C 3A7, Canada

E-mail: alexandre.zampa@grenoble-inp.fr

Received xxxxxx

Accepted for publication xxxxxx

Published xxxxxx

## Abstract

Inhomogeneous temperature elevations, also called hot spots, occurring in second generation high-temperature superconductor (2G HTS) tapes may lead to their destruction. A better understanding of inhomogeneous quenches would contribute to develop strategies to better protect superconducting devices based on 2G HTS tapes against hot spots. To do so, we investigated the current redistribution around a dissipative zone in a 2G HTS tape with a combination of experiments and numerical simulations based on the finite element method (FEM). Firstly, the inhomogeneous heat generation in a commercial 2G HTS bare tape (without copper cladding) was observed through the visualization of bubble generation. Secondly, the current redistribution around a dissipative zone in commercial 2G HTS bare tapes from two different manufacturers was investigated using voltage taps on both sides of the tape. The measured voltages showed that the current redistribution around the dissipative area in the top stabilizer layer of the tape is different from that in the bottom stabilizer layer. Using a 3D electro-thermal FEM model, we reproduced these behaviors, assuming a HTS tape architecture with an inhomogeneous local critical current density. Finally, using the same FEM model, we explored the impact of a lack of silver on one lateral side of a 2G HTS tape. Our results indicate that such a lack of silver does not critically affect the quench dynamics.

Keywords: 2G HTS, heterogeneous quench, modeling

## 1. Introduction

Second generation high-temperature superconductor (2G HTS) tapes show interesting properties such as high critical current density (even under high magnetic field), high maximum tensile stress, and low cryogenics costs thanks to their high critical temperature. They are well adapted to large scale applications.

One problem of 2G HTS tapes is the inhomogeneity of the critical current ( $I_c$ ) along their length combined with their low normal zone propagation velocity (NZPV). This makes them prone to localized thermal runaways, which may lead to high

temperature elevations, also called hot spots. This phenomenon is observed in many applications, such as resistive-type superconducting fault current limiters [1–4] or superconducting magnets [5]. The hot spot generally refers to a unique dissipative zone in the tape but an inhomogeneous heat dissipation with multiple dissipative zones preceding the complete quench of a tape is generally observed [6,7].

Several groups studied the behavior of 2G HTS tapes in the scenario of a hot spot. References [8,9] report experimental results that highlighted that the cross-section of two non-commercial 2G HTS tapes during inhomogeneous quenches is not at the same electric potential. At that time, the 2G HTS

tapes were not covered by stabilizer on the bottom side as well as on the lateral sides. Using a 2D model of a 2G HTS tape consisting of a nickel substrate, an YBCO layer, a silver layer and a copper layer, and considering the interfacial resistances between YBCO and nickel as well as YBCO and silver (no silver on the bottom side nor on the lateral sides), the different electric potential over the cross-section could be explained by a difference of interfacial resistances [10]. More precisely, due to a higher resistance at the YBCO/nickel interface than at the YBCO/silver interface, the current transfer from the HTS to the nickel occurred over a longer length than from the HTS to the silver. In [11], using a 3D model of a commercial 2G HTS tape that had stabilizer on the lateral sides and on the top and bottom of the tape, the current distribution around a hot spot was determined as a function of the thicknesses of the stabilizer on the top (HTS side) and bottom (substrate side) of the tape. The authors observed that the current distributions in the top and bottom stabilizer layers were very different even when they have identical thicknesses.

In this paper, we study the current density distribution and the temperature evolution in standard commercial 2G HTS tapes and we determine their spatial arrangements around a dissipative zone. Firstly, the optical observation of the bubble generation over the surface of a tape immersed in liquid nitrogen enabled us to observe the spread of the dissipative region along the tape width. Secondly, voltage measurements along the length of the sample and on the top and bottom stabilizer layers were carried out after the creation of a normal zone. Then, numerical simulations of the time evolution of the dissipation in the tape were carried out with a 3D model based on the finite element method (FEM) of a 2G HTS tape with an inhomogeneous critical current density. These simulations were compared with the experimental results. Finally, typical problem encountered in the stabilizer coming from the manufacturing process, such as lack of silver on the lateral sides, is investigated using the same 3D FEM model.

## 2. Observation of dissipative areas

### 2.1 Experimental details

Commercial 2G HTS tapes used in this work consisted of a 100  $\mu\text{m}$  thick substrate covered on the top side by a stack of buffer layers to enable the epitaxial growth of the HTS layer and to protect this layer from contamination by the substrate or the environment. This structure is surrounded by a thin stabilizer layer made of silver (see **Figure 1**). An additional copper layer can be electroplated depending on the application. In this work, samples from SuperPower [12] and SuperOx [13] were used. Their dimensions are given in Table I.

The observation of bubble generation on the surface of a 2G HTS tape is a powerful tool to identify locations where

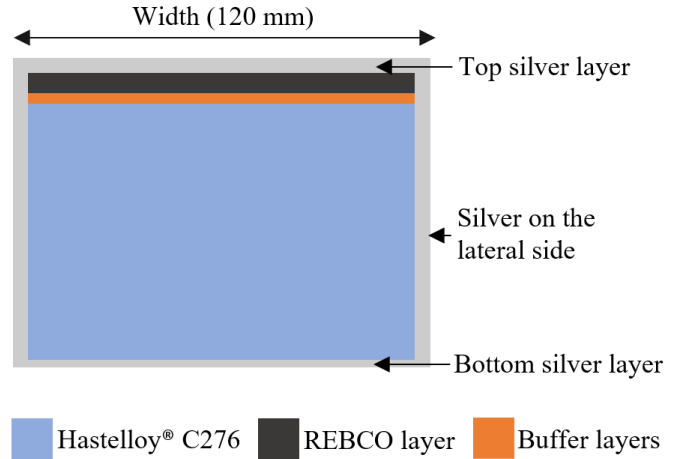


**Figure 1.** Schematic (not to scale) of the cross-section of a commercial 2G HTS tape.

dissipation occurs. The setup consists of a transparent cryostat filled with liquid nitrogen at 77 K, where a 12 mm wide and 65 mm long 2G HTS tape from Superpower ( $I_c(77\text{ K})\sim 500\text{ A}$ ) was immersed and connected to a DC electric circuit shown in **Figure 2**. This DC circuit has been used to initiate the thermal runaway of the 2G HTS tape sample. The voltage source  $V_{\text{source}}$  was based on a supercapacitor (Maxwell 165 F-48 V), whose capacity was big enough to ensure negligible voltage drop over time. The current flowing in the sample, during the total duration of the tests, was interrupted after 10 ms by a switch S composed of five MOSFETs in parallel. The circuit impedances  $R_{\text{circuit}}$  and  $L_{\text{circuit}}$  were determined experimentally and are given in Table II. A 1,000 A current clamp was used to measure the current. A high-speed Phantom V311 camera able to record one image every 20  $\mu\text{s}$  was used to observe the bubble generation on the surface of the sample. More details are given about the experimental setup in [7].

TABLE I  
Dimensions of some 2G HTS tapes

Manufacturers	SuperOx	Superpower
Substrate thickness ( $\mu\text{m}$ )	100	100
Buffer layers thickness ( $\mu\text{m}$ )	0.4	0.2
REBCO thickness ( $\mu\text{m}$ )	1.5	1
Top stabilizer layer ( $\mu\text{m}$ )	2	2
Bottom stabilizer layer ( $\mu\text{m}$ )	1	1.8
Lateral side stabilizer thickness ( $\mu\text{m}$ )	1	1

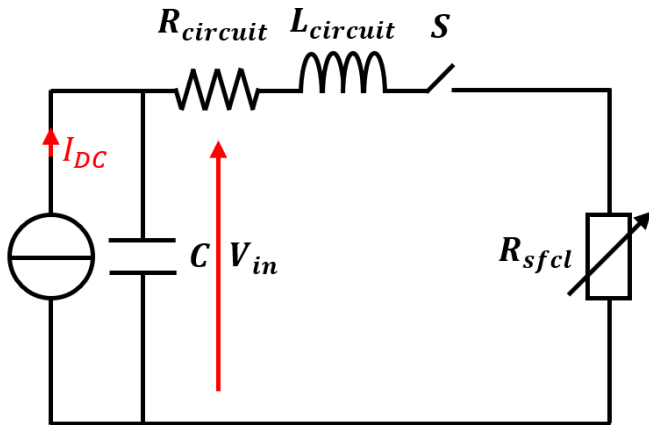


**Figure 2.** Electric circuit used to initiate a thermal runaway in the tape.

TABLE II  
Parameters of the circuit

$V_{\text{source}}$ (V)	$R_{\text{circuit}}$ ( $\Omega$ )	$L_{\text{circuit}}$ ( $\mu\text{H}$ )
18	0.022	3.5

## 2.2 Results

**Figure 3** presents the images obtained during the very beginning of a thermal runaway occurring in the SuperPower sample for a prospective current of 815 A. The time  $t=0$  corresponds to the application of the transport current. Two different dissipation behaviors leading to the formation of the dissipation columns A and B are presented in the figure. The formation of column A starts locally at 0.72 ms (corresponding to the first bubble observed). Then, it rapidly expands across the width of the sample, perpendicularly to the current path, to form a fully developed dissipation column at 0.90 ms. The propagation then continues more slowly in the longitudinal direction of the tape. The behavior of dissipation column B is different. It starts at around 0.84 ms at two different locations that are shifted along the longitudinal axis of the tape. The two dissipation areas expand along the width until they meet at 1.24 ms. Then, the dissipation column propagates along the longitudinal direction of the tape.

A similar evolution of a dissipation spot was also mentioned in [13]. Furthermore, in [7], it was shown that areas with low superconducting properties in a 2G HTS tape (determined with Scanning Hall Probe Microscopy) matched the positions of the dissipation columns.

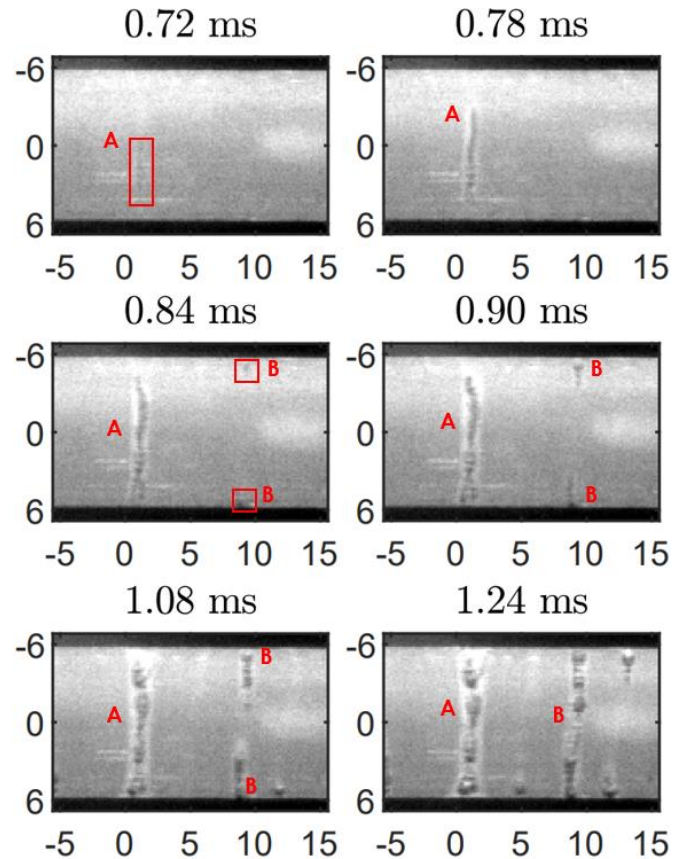


**Figure 3.** Images of the bubble generation over the surface of a 12 mm wide Superpower sample immersed in a liquid nitrogen bath. Letters A and B refer to the two dissipation columns discussed in this paper. On the axes, 0 refers to the center of the tape in mm along the length (x-axis) and width (y-axis)

## 3. Electrical measurements around a dissipation spot

### 3.1 Description of the setup

Electrical measurements were performed on a 12 mm wide and 60 mm long 2G HTS tape from SuperOx [14] ( $I_c(77\text{ K}) \sim 700\text{ A}$ ), whose cross-section is detailed in **Figure 1** and its dimensions are given Table I. Twelve voltage taps were soldered on the stabilizer using indium-tin solder. The taps were placed 1 cm apart along the length of the tape, symmetrically on the top and bottom sides (see **Figure 4**). A small permanent magnet was positioned in the middle of longitudinal direction the sample to locally decrease the critical current and generate the initial normal zone.

Pressed current contacts (copper blocks) were used to connect the sample with the electric circuit presented in

TABLE III  
Parameters of the circuit

$V_{\text{source}}$ (V)	$R_{\text{circuit}}$ ( $\Omega$ )	$L_{\text{circuit}}$ ( $\mu\text{H}$ )
18	0.027	3.8

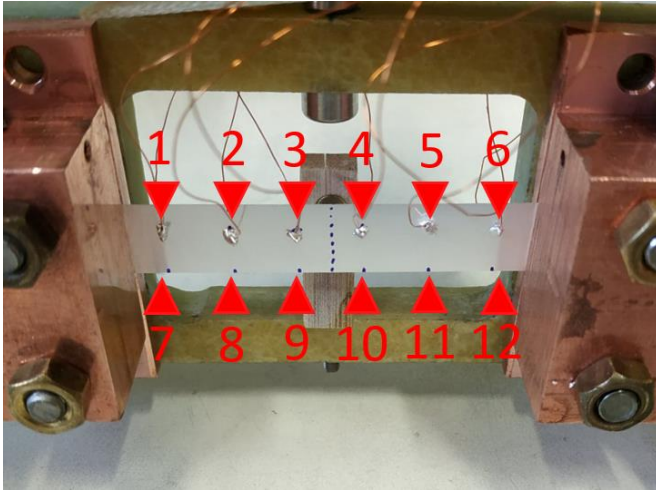


**Figure 4.** Picture of the sample equipped with six voltage taps on the HTS side (from 1 to 6) and on the substrate side (from 7 to 12).

**Figure 2**, whose parameters are given in Table III. The prospective current was 665 A.

### 3.2 Results

**Figure 5** shows the current and voltages measured when the applied current is higher than the critical current at the magnet location, but lower than the critical current of the tape away from the magnet. Firstly, we observe that voltages measured on the bottom side of the stabilizer (substrate side), *i.e.*  $V_{7,8}$ ,  $V_{8,9}$ ,  $V_{9,10}$ ,  $V_{10,11}$  and  $V_{11,12}$ , all appear simultaneously at 4 ms. The voltage is lower on the portions of the sample far from the defect location, where the thermal runaway is initiated. On the top side of the stabilizer (HTS side), only the voltage measured between voltage taps 3 and 4 ( $V_{3,4}$ ) is different than zero.

These results indicate a difference in the current transfer lengths occurring between i) the top stabilizer layer and the HTS layer, and ii) the bottom stabilizer layer and the HTS layer. In other words, the current circulates along a wider zone in the stabilizer layer located at the bottom of the tape. Furthermore, from the amplitude of the measured voltages, we deduce that the current density in the bottom stabilizer layer gradually increases as we approach the defect and reaches its maximum at the defect location. We also note that the voltages are not identical with respect of the center of the tape. This may come from imperfections in voltage taps spacing.

Similar results, not presented in this paper, were experimentally obtained on a 2G HTS tape from another manufacturer (Superpower).

## 4. Simulation of a dissipation spot

A 3D finite-element model (FEM) built with COMSOL Multiphysics was used to recreate the dissipation observed in section 2 and to simulate the experiments described in

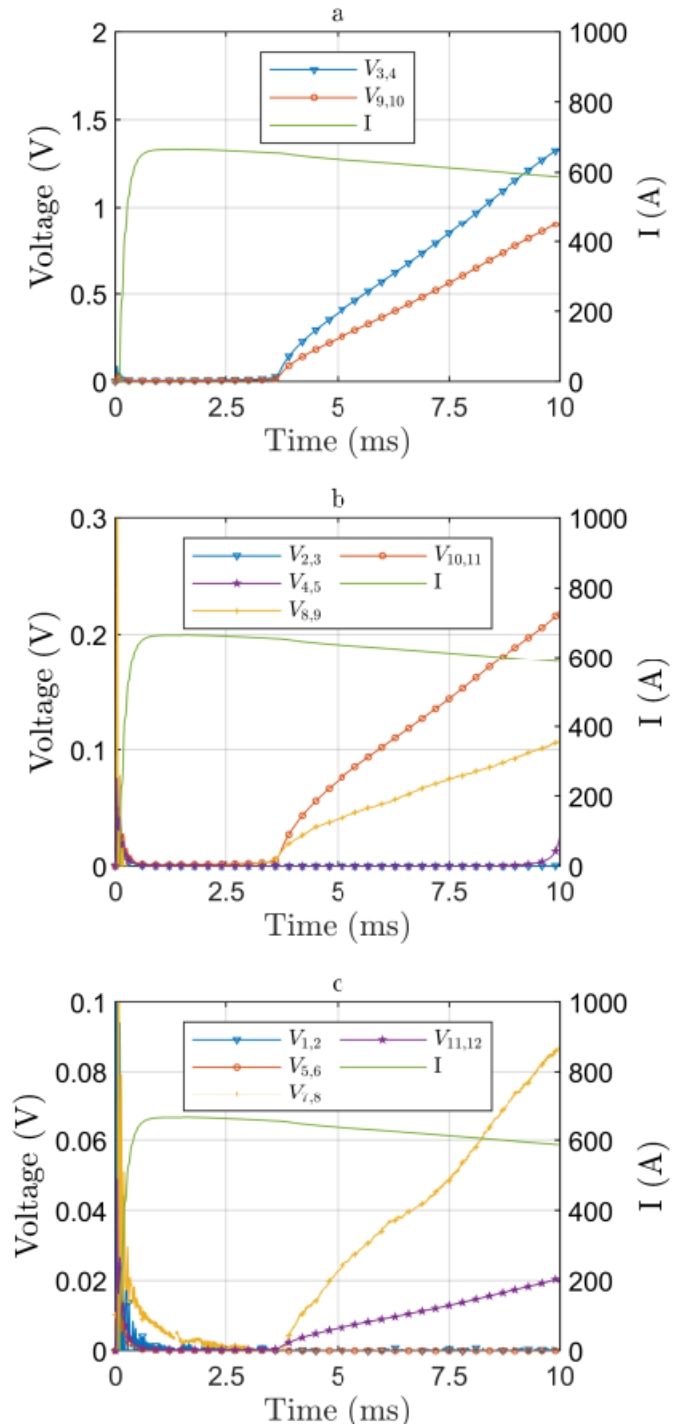


**Figure 5.** Voltages measured on the SuperOx sample as a function of the time (lines with symbols). The current in the circuit as a function of the time is also given (green solid line).

section 3 in order to visualize the current redistribution in the stabilizer layer.

### 4.1 Model of 2G HTS tape

Details of the model can be found in [15]. Here, we only summarize the main features of the model to understand how

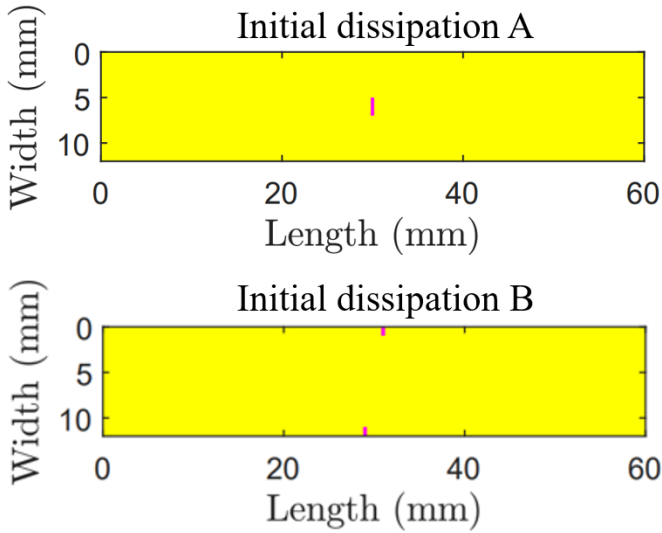


**Figure 6.** Critical current density distributions used in the simulations where  $J_c = 3.35 * 10^{10}$  A/m<sup>2</sup> in the yellow part and  $J_c = 0.335 * 10^{10}$  A/m<sup>2</sup> in the purple areas. The top  $J_{c,0}$  distribution was used to reproduce the evolution of column A in Figure 3, while the bottom  $J_{c,0}$  distribution was used to reproduce the evolution of column B in Figure 3.

the simulation results are obtained. All simulations were carried out for 10 ms at 77 K.

#### 4.1.1 Geometry and materials

A 6 cm long SuperOx tape, as in **Figure 1** with the dimensions given in Table I, was modelled. Note that the stack of buffer layers was not modeled as a volume element but rather as an insulating interface (2D element). The heat capacity per unit volume, the resistivity and the heat conductivity were taken from [16,17].

The REBCO layer is electrically modeled assuming two resistances in parallel giving the electrical conductivity  $\sigma_{\text{rebco}}$  given by (1), where  $\sigma_{\text{sc}}$  is the electrical conductivity of the material in the superconducting state, and  $\sigma_{\text{nsc}}$  is the electrical conductivity at the normal state. The electrical conductivity  $\sigma_{\text{sc}}$  follows the power law given by (2), where  $E$  is the norm of the electric field,  $E_c$  denotes the electric field criterion,  $J_c$  is the critical current density with the dependence in temperature given by (3). The  $n$ -value is given by (4), which comes from experimental measurements.

$$\sigma_{\text{rebco}} = \sigma_{\text{sc}} + \sigma_{\text{nsc}} \quad (1)$$

$$\sigma_{\text{sc}} = \frac{J_c(T)}{E} \left( \frac{E}{E_c} \right)^{\frac{1}{n(T)}} \quad (2)$$

$$J_c(T) = \begin{cases} J_{c,0} \frac{(T - T_c)}{77 - T_c}, & T < T_c \\ 0, & T \geq T_c \end{cases} \quad (3)$$

$$n(T) = 0.37T + 15.8 \text{ with } T < T_c \quad (4)$$

Two different critical current density distributions  $J_{c,0}$  were considered. Each current density distribution was

implemented to reproduce the initial dissipation areas A or B observed in **Figure 3**. In the first distribution, see **Figure 6 (top)**, the tape has a uniform critical current density with one 400  $\mu\text{m}$  long and 2 mm wide single defect that was used to reproduce the evolution of column A. In the second distribution of **Figure 6 (bottom)**, two 400  $\mu\text{m}$  long and 1 mm wide defects located at slightly different positions along the sample length were used to simulate the evolution of column B.

The critical current density of the tape away from the defects (in the yellow parts) was adjusted to obtain an initiation of the thermal runaway at the same time as it occurred experimentally in section 3.

#### 4.1.2 COMSOL Multiphysics modules

**Electric currents and electric circuit** - The tape is connected to a circuit as the one described in **Figure 2** using the parameters given in Table III. The current can flow in all layers except the buffer layers, which is modeled as an insulator and do not have a thickness in the model.

**Heat transfer in solids** - The temperature at the tape extremities, i.e. at positions 0 mm and 60 mm along the length, was fixed at 77 K, which corresponds to the temperature of the liquid nitrogen bath. The heat transfer between the tape and the liquid nitrogen bath was not considered in the simulations i.e. the tape is in adiabatic conditions.

#### 4.1.3 Voltages probes

Virtual voltage probes were inserted in the model to follow the evolution of the voltage on the top and bottom stabilizer layers of the tape. The voltage probes were positioned in the same way as described in the experiment (see **Figure 4**).

#### 4.2 Inhomogeneous dissipation along the width

The first objective of the simulations was to simulate the heat dissipation observed experimentally and discussed in section 2.

##### 4.2.1 One single defect – Initial dissipation A

In **Figure 7**, we present the calculated temperature on the top of a tape at different times of the simulation in the case of a single defect. We observe that the heat first propagates along the width of the tape, starting from the defect and moving towards the sides of the tape. This is an evolution similar to what was observed experimentally (column A).

In **Figure 8**, we present the calculated current density in the superconducting layer in the case of a single defect at different time instants. At the longitudinal position of the defect ( $x = 30$  mm), we observe that the current density is higher in the volume surrounding the defect. Indeed, the low critical current

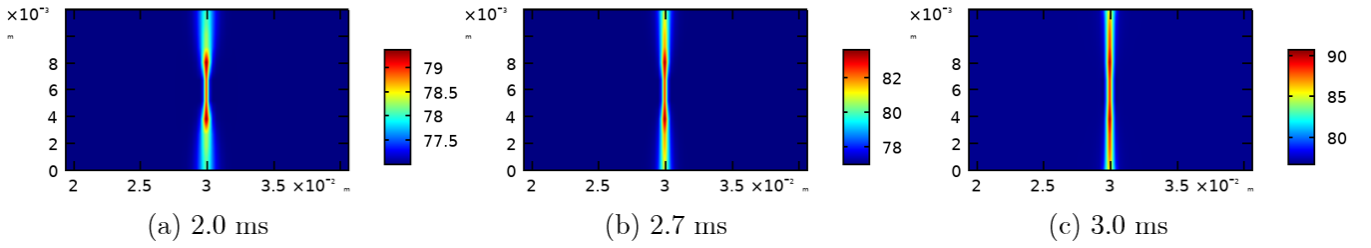


**Figure 7.** Temperature on the top stabilizer layer of the tape at different times during the simulation in the case of a single defect (zoom between  $x = 2$  cm and  $x = 4$  cm).

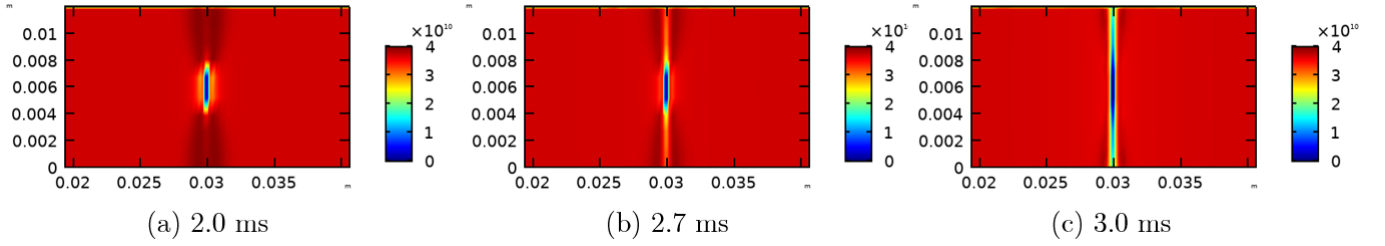


**Figure 8.** Current density in the superconducting layer (in the center of the thickness on the  $z$ -direction) at different times during the simulation in the case of a single defect (zoom between  $x = 2$  cm and  $x = 4$  cm).

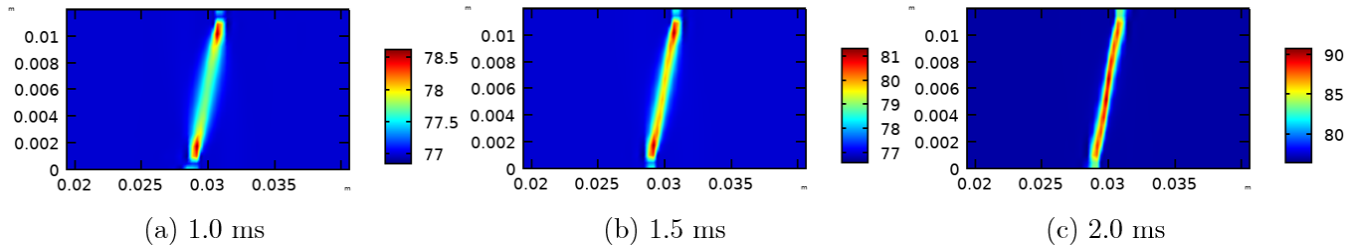


**Figure 9.** Temperature on the top stabilizer layer of the tape at different times during the simulation in the case of two distinct defects (zoom between  $x = 2$  cm and  $x = 4$  cm).

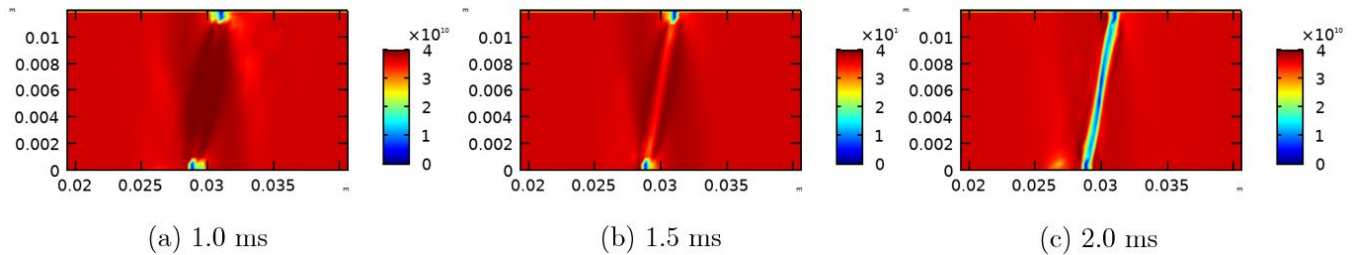


**Figure 10.** Current density in the superconducting layer (in the center of the thickness on the  $z$ -direction) at different times during the simulation in the case of two distinct defects (zoom between  $x = 2$  cm and  $x = 4$  cm).

at the defect location (purple areas in **Figure 6**) forces the current to flow around it. The higher current density in this area compared to the rest of the tape initiates a local dissipation starting at the border of the defect which furthermore increases the current density in the rest of the tape width. The current density in the superconducting layer, at the longitudinal position of the defect, gradually decays and starts to share with the other electrically conductive layers until the dissipating area reaches the edges of the tape. Once the tape

has quenched across the entire width, the current does not flow anymore in the superconducting layer at the defect location, it flows through the stabilizer and the substrate (see **Figure 8c**).

#### 4.2.2 Two distinct defects – Initial dissipation B

The time evolution of the temperature on the top stabilizer layer in the case of a current density distribution with two defects (see **Figure 6**) is presented in **Figure 9**. We observe that the temperature increases in the immediate vicinity of the

defects. The heat then propagates along a straight line between the two defects. This case reproduces very well what was observed in Figure 3, where the dissipation column B is not perfectly parallel with the direction of the width.

In Figure 10, the current density is presented. We observe that, at the very beginning of the simulation, the current density increases between both defects and is at its highest value near the defects (see Figure 10a). These initiates heat generation and contributes to reduce the effective cross-section of superconductor. The reduction of the superconducting area where the current can flow in continues until the cross-section between the two defects is sufficiently hot to force current sharing with the other layers (see Figure 10c). The evolution of either the temperature or the current density in the superconducting layer highlights a normal zone propagation first occurring in the width direction.

On one hand, the numerical simulations give the temperature elevation. On the other hand, the observation of the bubble generation helps identify the locations of temperature elevations in the tape. The bubble generation is a consequence of the temperature elevation. A difference of temperature is required between the tape surface and the liquid nitrogen bath to initiate bubble generation [18]. It is however difficult to know precisely at which temperature bubble generation starts. As a consequence, the simulation results can only be qualitatively compared to the measurements.

#### 4.3 Inhomogeneous dissipation along the length

Here, we investigate the current redistribution around a dissipation column in the case of one single defect and we compare the numerical results with the experimental results presented in section 3.

##### 4.2.1 Time evolution of voltages and current

Since the results on each side of the defect (located at the center of the sample) are symmetrical, only the results on one side of the tape are shown.

Figure 11 shows that the simulation results are qualitatively similar to the experimental results. The simulated voltages drop in portions 7-8, 8-9, 9-10, located on the bottom side of the stabilizer, all appear simultaneously at 4 ms, while on the top side of the stabilizer, only the voltage on portion 3-4 becomes visible. Similarly as in the experiments, the calculated voltage on the bottom side decreases as the probe moves away from the center of the tape.

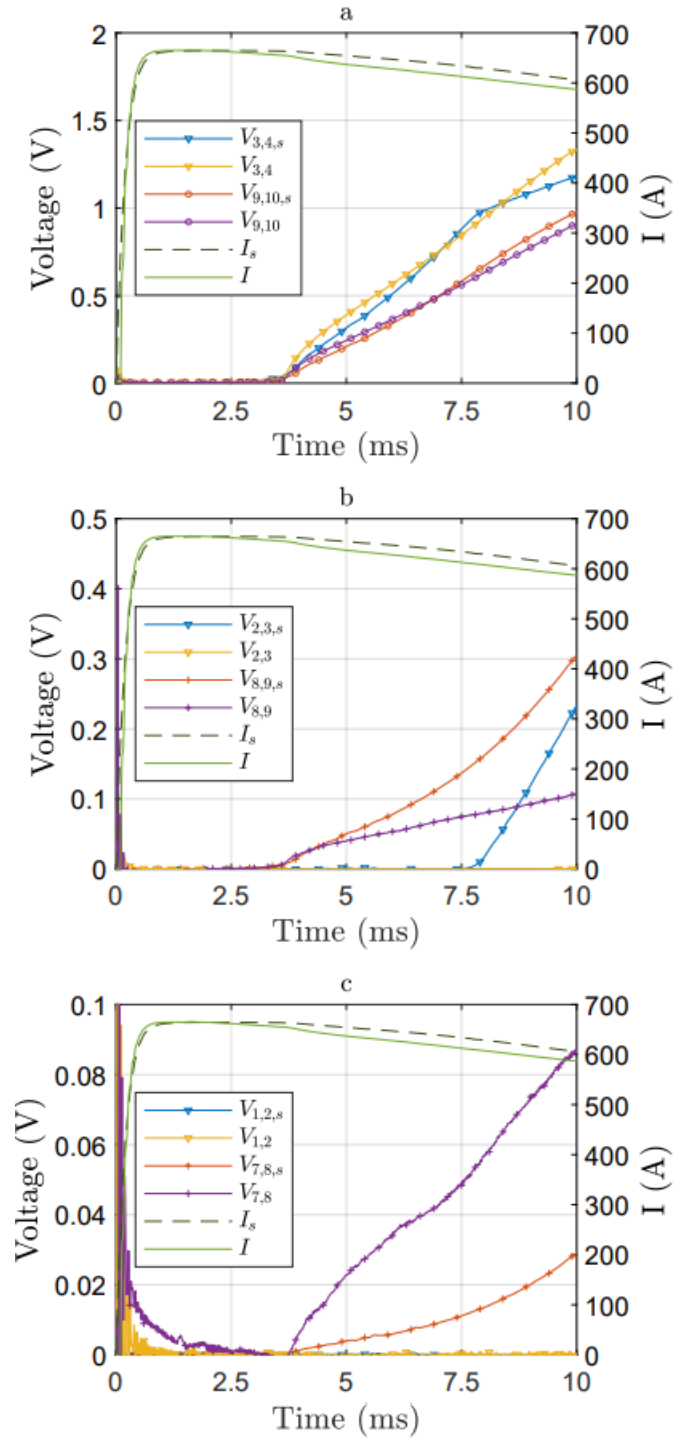


**Figure 11.** Comparison of simulated and measured voltages vs. time in different portions of the tape on the top and bottom stabilizer layers. The “s” subscript identifies curves obtained by numerical simulations. The measured voltages are from Figure 5 and are obtained on a SuperOx tape.

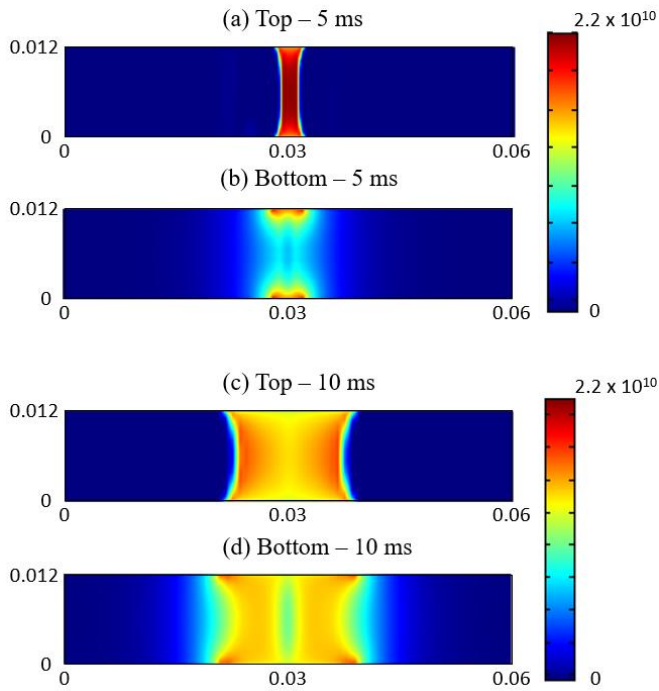


**Figure 12.** Current density in the top and bottom stabilizer layers at 5 ms and 10 ms. The units of the x and y axes are millimeters.

However, even if simulations and experiments qualitatively agree, the voltages are not identical. Indeed, in Figure 11b, we see that the calculated voltage  $V_{2,3, \text{simu}}$  starts to increase at 8 ms, while the corresponding measured voltage  $V_{2,3}$  is still zero. Note that the model does not consider the interface resistances between the superconducting layer and the other conductive layers as well as the convective heat transfer from the tape to the liquid nitrogen. In addition, the resistivity of the stabilizer comes from [16] while these values can sensibly deviate from the actual resistivity of the SuperOx tape. Imperfections in the voltage taps spacing in the experiment may also contribute to the differences observed.

These differences in the voltages between the top and bottom stabilizer layers observed in the experiments and in the simulations highlight the differences in the current distribution between the top and bottom stabilizer layers. **Figure 12** presents the current density on the surface of the top and bottom stabilizer layers. We observe that the current flows over a larger zone in the bottom stabilizer layer than in the top stabilizer layer. The difference of current distribution between the bottom stabilizer layer and the top stabilizer layer is explained by a more resistive path between the HTS layer and the bottom stabilizer layer than between the HTS layer and the top stabilizer layer. Similar results were predicted using a 2D electrical modelling in [10].

#### 4.2.2 Temperature

The temperatures on the top and bottom surfaces of the tape are shown in **Figure 13**. The heat propagation fronts are

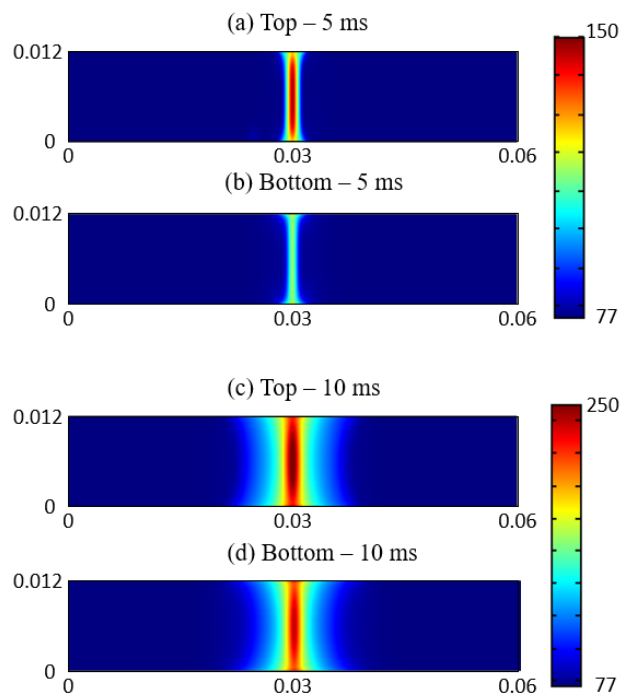


**Figure 13.** Surface temperature on the top and bottom stabilizer layers at 5 ms and 10 ms. The units of the x and y axes are millimeters.

almost identical on the top and bottom stabilizer layers even if the current distributions are not. This is not surprising due to the low thickness of the tape. However, we note that the temperature distribution is not identical across the width. As explained in Reference [11], this is due to the current that flows through the lateral sides of the tape to reach the bottom stabilizer layer. The current density in the lateral side becomes higher than in the rest of the tape (see **Figure 12b**), which leads to a higher temperature on the edges. A similar pattern was experimentally observed on a 2G HTS tape during an inhomogeneous quench in [19]. It was observed that the bubbles created from the heat dissipation had the shape of a hourglass.

## 5. Influence of the lack of stabilizer on the lateral sides

Section 4 highlighted the importance of the stabilizer on the lateral sides to enable the circulation of the current from the HTS layer to the bottom stabilizer layer, resulting in a larger

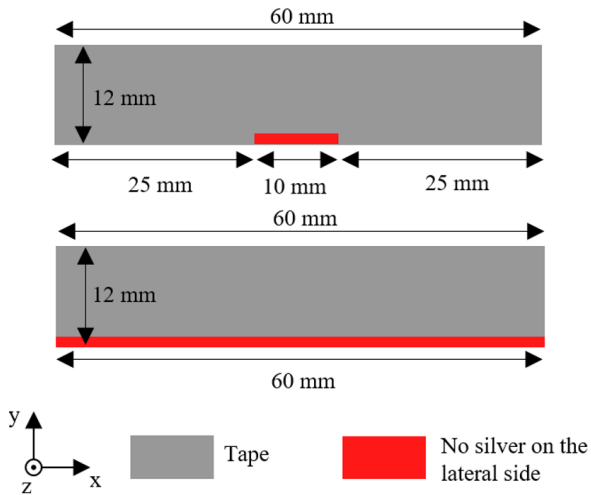


**Figure 14.** Top view of a tape with a lack of silver: 1) over a length of 1 cm on one lateral side of the tape, and 2) totally removed on one lateral side of the tape.

current transfer length than when current transfers from the HTS layer to the top stabilizer layer.

It is known that partial lack of stabilizer may occur on the lateral sides of the tape. This may impact the safe operation of the tape due to the circulation of the current through the lateral sides. This section investigates this possible issue.

### 5.1 Description of the model

The same model as that described in section 4.1 was used, with the difference that stabilizer is locally removed over a length of 1 cm or entirely removed on one lateral side of the tape (see **Figure 14**).

### 5.2 Results

**Figure 15a** shows the temperature of a tape at 5 ms in the case of a complete coverage of stabilizer (no lack of silver). It is compared with the cases of a 1 cm long lack of stabilizer on one lateral side (**Figure 15b**) and a 6 cm long lack of stabilizer on one lateral side (**Figure 15c**). The maximum temperature in the whole volume of the tape, at the end of the simulation, reaches 272 K in the case of the 6 cm long lack of stabilizer, 257 K in the case of the 1 cm lack of stabilizer and 251 K with no lack of silver. We can conclude that the lack of stabilizer does not induce a huge difference in the hot spot temperature (increase of 21 K in the case of the 6 cm long lack of however).

**Figure 16** presents the current density in the  $y$ -direction (along the width) in the top and bottom stabilizer layer. We observe that the component of the current density along the width in the bottom stabilizer is more important when the silver is totally removed from one lateral side. This indicates that even if the lack of stabilizer increases the current transfer length (i.e. the length of tape necessary to transfer the current from the superconducting material to the stabilizer), it does not significantly affect the current density, which justifies the

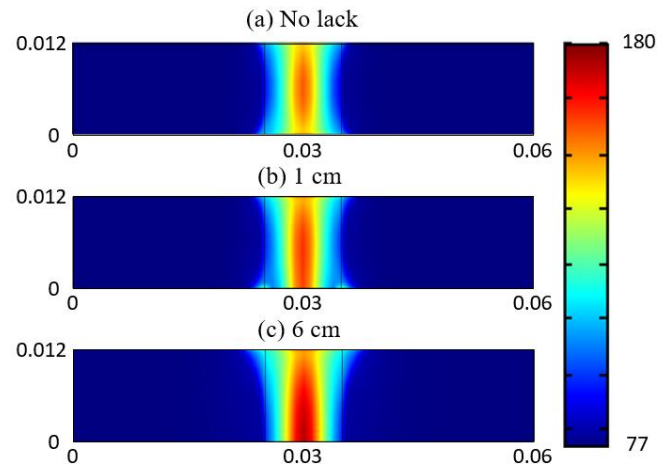


**Figure 15.** Temperature of the top stabilizer layer at 5 ms with (a) complete covering of the lateral sides with stabilizer (b) a lack of stabilizer over a length of 1 cm (c) a lack of stabilizer over a length of 6 cm.

relatively small temperature elevation. We can conclude that a lack of silver on one lateral side of a tape is not ideal but it should not affect drastically the good operation of a commercial tape.

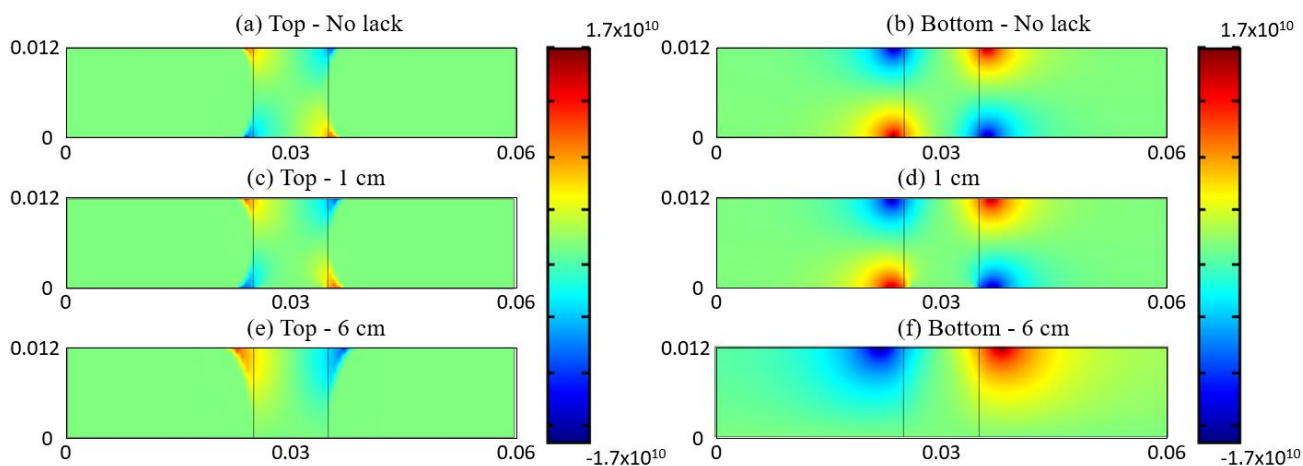


**Figure 16.** Component of the current density in the  $y$ -direction (width) on the top and bottom surfaces of the tape at 5 ms with (a)-(b) a complete covering of the lateral side by stabilizer, (c)-(d) with a 1-cm long lack and (e)-(f) with a 6 cm lack of stabilizer.

## Conclusion

In this paper, we investigated the electro-thermal behavior of a tape during the formation of a dissipative zone. The results from numerical simulations coupled with experiments showed that the dissipation starts in the direct vicinity of a defect due to current crowding since the amount of current flowing in the defect area(s) is reduced. Over time, the dissipation area first propagates across the width of the tape to form a dissipation column. Then, the dissipation area propagates in the longitudinal direction of the tape. The current distribution around this dissipation area is different in the top and bottom stabilizers, leading to a cross-section of the tape not showing the same electric potential.

Overall, the results presented in this work give a better understanding of the current path in presence of defects, which allow one to anticipate possible issues (or non-issues) occurring in 2G HTS tapes during a quench. For instance, it was shown that a lack of stabilizer on the lateral side of a tape increases moderately the temperature elevation in the tape. In the past, the study of the current redistribution from the superconducting material to the conductive layers made it possible to develop the concept of Current Flow Diverter [11] to promote the normal zone propagation. This paper could open new ways to improve the protection of technologies such as Superconducting Fault Current Limiter or Insulated coils by the addition of knowledge about the current redistribution around a defect area.

## Acknowledgements

Thank you to A. Derby & B. Sarrazin for the development of the DC switch.

## References

[1] Tixador P, Nguyen-Nhat T, Okada-Vieira H G and Ponceau R 2011 Impact of Conductor Inhomogeneity on FCL

Transient Performance *IEEE Trans. Appl. Supercond.* **21** 1194–7

- [2] Colangelo D and Dutoit B 2012 Inhomogeneity effects in HTS coated conductors used as resistive FCLs in medium voltage grids *Supercond. Sci. Technol.* **25** 095005
- [3] de Sousa W T B, Kudymow A, Strauss S, Palasz S, Elschner S and Noe M 2020 Simulation of the Thermal Performance of HTS Coated Conductors for HVDC SFCL *J. Phys.: Conf. Ser.* **1559** 012097
- [4] Gömöry F and Šouc J 2021 Stability of DC transport in HTS conductor with local critical current reduction *Supercond. Sci. Technol.* **21**
- [5] Badel A, Rozier B, Ramdane B, Meunier G and Tixador P 2019 Modeling of ‘quench’ or the occurrence and propagation of dissipative zones in REBCO high temperature superconducting coils *Supercond. Sci. Technol.* **32** 094001
- [6] Nguyen N T and Tixador P 2010 A YBCO-coated conductor for a fault current limiter: architecture influences and optical study *Supercond. Sci. Technol.* **23** 025008
- [7] Zampa A, Holleis S, Badel A, Tixador P, Bernardi J and Eisterer M Influence of local inhomogeneities in the REBCO layer on the quench mechanism of 2G HTS tapes *Submitted in August 2021*.
- [8] Duckworth R C, Lue J W, Lee D F, Grabovickic R and Gouge M J 2003 The role of nickel substrates in the quench dynamics of silver coated YBCO tapes *IEEE Trans. Appl. Supercond.* **13** 1768–71
- [9] Wang X, Caruso A R, Breschi M, Zhang G, Trociewitz U P, Weijers H W and Schwartz J 2005 Normal Zone Initiation and Propagation in Y-Ba-Cu-O Coated Conductors With Cu Stabilizer *IEEE Trans. Appl. Supercond.* **15** 2586–9
- [10] Breschi M, Ribani P L, Wang X and Schwartz J 2007 Theoretical explanation of the non-equipotential quench

- behaviour in Y–Ba–Cu–O coated conductors *Supercond. Sci. Technol.* **20** L9–11
- [11] Lacroix C, Sirois F and Lupien J-H F 2017 Engineering of second generation HTS coated conductor architecture to enhance the normal zone propagation velocity in various operating conditions *Supercond. Sci. Technol.* **30** 064004
- [12] Selvamanickam V, Chen Y, Xiong X, Xie Y Y, Reeves J L, Zhang X, Qiao Y, Lenseth K P, Schmidt R M, Rar A, Hazelton D W and Tekletsadik K 2007 Recent Progress in Second-Generation HTS Conductor Scale-Up at SuperPower *IEEE Transactions on Applied Superconductivity* **17** 3231–4
- [13] Heinrich A Quenching of superconductivity and propagation of the resulting normal phase in YBCO films 7
- [14] Anon <https://eng.s-innovations.ru>
- [15] Lacroix C and Sirois F 2014 Concept of a current flow diverter for accelerating the normal zone propagation velocity in 2G HTS coated conductors *Supercond. Sci. Technol.* **27** 035003
- [16] David L 1993 *Crc handbook of chemistry and physics: a ready reference of chemical and physical data 74th ed* (Journal of the American Chemical Society)
- [17] Lu J, Choi E S and Zhou H D 2008 Physical properties of Hastelloy<sup>®</sup> C-276<sup>TM</sup> at cryogenic temperatures *Journal of Applied Physics* **103** 064908
- [18] Sakurai A, Shiotsu M and Hata K 1990 Effect of System Pressure on Minimum Film Boiling Temperature for Various Liquids *Experimental Thermal and Fluid Science* **3** 8
- [19] Zampa A, Tixador P and Badel A 2021 Experimental Observations of the Hot-Spot Regime On 2G HTS Coated Conductors *IEEE Transactions on Applied Superconductivity* **31** 1–5